# Sheffield Hallam University

# Bicontinuous minimal surface nanostructures for polymer blend solar cells

KIMBER, R. G. E., WALKER, A. B., SCHRODER-TURK, G. E. and CLEAVER, D. J. <http://orcid.org/0000-0002-4278-0098>

# Bicontinuous minimal surface nanostructures for polymer blend solar cells

Robin G. E. Kimber[*]     Alison B. Walker[†]

Gerd E. Schröder-Turk[‡]     Douglas J. Cleaver[§]

October 2, 2009

## Abstract

This paper presents the first examination of the potential for bicontinuous structures such as the gyroid structure to produce high efficiency solar cells based on conjugated polymers. The solar cell characteristics are predicted by a simulation model that shows how the morphology influences device performance through integration of all the processes occurring in organic photocells in a specifed morphology. In bicontinuous phases, the surface defining the interface between the electron and hole transporting phases divides the volume into two disjoint subvolumes. Exciton loss is reduced because the interface at which charge separation occurs permeates the device so excitons have only a short distance to reach the interface. As each of the component phases is connected, charges will be able to reach the electrodes more easily. In simulations of the current-voltage characteristics of organic cells with gyroid, disordered blend and vertical rod (rods normal to the electrodes) morphologies, we find that gyroids have a lower than anticipated performance advantage over disordered blends, and that vertical rods are superior. These results are explored thoroughly, with geminate recombination, i.e. recombination of charges originating from the same exciton, identified as the primary

[*]Department of Physics, University of Bath, Bath, BA2 7AY, UK

[†]Department of Physics, University of Bath, Bath, BA2 7AY, UK Email: `a.b.walker@bath.ac.uk`

[‡]Institut für Theoretische Physik, Friedrich-Alexander Universität, Erlangen-Nürnberg, Staudtstraße 7, D-91058 Erlangen, Germany

[§]Materials and Engineering Research Institute, Sheffield Hallam University, Howard Street, Sheffield, S1 1WB, UK

source of loss. Thus, if an appropriate materials choice could reduce geminate recombination, gyroids show great promise for future research and applications.

## Introduction

Organic photovoltaics have the potential to produce cheap solar power in lightweight, flexible and portable cells.[1,2] Compared to their inorganic counterparts, organic cells are a relatively new technology, with several issues still to be addressed before becoming commercially viable. There are several types of organic cells: hybrid organic/inorganic cells,[3] and all-organic cells such as conjugated polymer-fullerene composites with power conversion efficiencies exceeding 5%,[4–6] and conjugated polymer blend cells with efficiencies as high as 1.8%.[7,8]

In polymer blend solar cells, absorbed photons generate excitons, which dissociate into electron-hole pairs at the interface between the two polymers, which are then extracted by the electrodes to create a photocurrent. The morphology of the active layer of organic photovoltaics at the nanoscale is of great interest, as it impacts strongly on device performance.[2] Due to the low exciton diffusion length, around 10-20 nm,[2] compared to the optical absorption length, typically 100 nm, a bulk heterojunction morphology that employs an interpenetrating network of the component polymers is frequently employed. A finely intermixed morphology with small feature sizes is best for exciton dissociation, however, a coarse morphology is required for collection of the photogenerated charges. There is therefore a tradeoff between these two processes as has been demonstrated by Dynamical Monte Carlo (DMC) simulations that we adapted from surface physics to look at charge and energetic processes in any morphology on the nanometre scale.[9] Since our original work, DMC has been used as a general investigation of morphology,[10–12] or to examine specific loss mechanisms.[13,14]

**Drift-diffusion modelling has also been successfully used to model organic solar cells.[15–17] However, such models are unable to take full account of the effect of three-dimensional structures, which are of interest here, instead reducing the complex morphology to a homogeneous system or a simplified two-dimensional**

**structure. These models, apart from,[17] also do not normally take full account of the related process of exciton dissociation, which has multiple stages that are critically influenced by morphology.[13,18]**

The blend structures used in solar cells are in general highly disordered and are prone to the development of disconnected islands which limit charge collection. Thus, the identification of routes to more efficient structures, as well as a greater understanding of loss mechanisms, is highly desirable. Self-assembling ordered microphase-separated geometries such as the gyroid morphology can be seen in diblock copolymers[19] and certain dendrimer systems.[20] In principle, such systems should yield improved phase connectivity when compared with the basic percolation pathways offered by random blends. The observation that such phases can freely self-assemble from systems as simple as appropriately-shaped hard particles[21] indicates that there is no length-scale limitation on the periodicities of these phases. We speculate, therefore, that there are no fundamental materials problems that would prevent realisation of a hybrid solar cell device based on a gyroid morphology.

These bicontinuous morphologies have a large interfacial area and continuous transport pathways, and the generation of morphologies by self-assembly makes such structures highly reproducible.[22] Gyroid morphologies have been created in nanoporous films by, amongst others, Urade et al.[23] Bulk heterojunction solar cells made from a porous titania structure synthesised using a poly(styrene-block-polyethylene oxide) diblock copolymer template infiltrated with a semiconducting polymer were made by Oey et al,[24] who noted that gyroid structures could be created by this technique. Recently, gyroid and columnar structures were replicated in anatase titania and the titania structures immersed in dye and back filled with a liquid electrolyte to create dye-sensitised cells (DSCs).[25,26] These cells show power efficiencies of around 2%, considerably less than the best efficiencies of 11% obtained for liquid electrolyte dye-sensitised cells made from mesoporous titania,[27] but comparable to devices of a similar thickness. To the authors' knowledge, **such bicontinuous structures** have yet to be adopted in an all-conjugated polymer solar cell, although diblock copolymers based on conjugated polymers have now been synthesised.[28]

Here, we present the results of DMC simulations of polymer solar cells employing a range of morphology classes. We examine three bicontinuous morphologies, as formed in diblock copolymers: the gyroid, double gyroid and double diamond phases. We assess the feasibility of these structures on different length scales as novel active layer morphologies, in comparison to two other classes: the disordered blend and interdigitated vertical rod morphologies. The interdigitated structure used is similar to the cylindrical phase, which can also form in such materials.[29] These structures are illustrated in 1. To date, nearly all the reported DMC simulations have only looked at short-circuit, and been limited to a small range of morphologies. Here, we extend DMC to open-circuit, and separately examine geminate and bimolecular recombination, and the impact of high illumination.

**The polymer backbone in conjugated polymers may be too rigid for a gyroid phase to form, and to date it is yet to be observed.[30,31] S. Sun has suggested the use of a flexible non-conjugated bridge unit in order to overcome this problem.[32] However, our emphasis here is on the usefulness of bicontinuous structures due to the recent interest in such structures, and the possibility that these structures could be made in the near future. All three structures studied here share the essential traits of island-free continuous charge transport pathways with a high interfacial area, which should provide a clear performance improvement on existing disordered blend structures.**

## Model

Within each morphology class, a range of morphologies with different feature sizes have been created. The feature size $l_f = 3r_{VS}$, where $r_{VS}$ is the volume-to-surface ratio,[10] provides a rough approximation for the average domain sizes. While more direct measures for domain size are available,[33–36] the method used here is sufficient to identify performance trends. The solar cell is modelled by $64 \times 64 \times 64$ voxels each of dimensions 1 nm$^3$ where each voxel represents a hopping site. Periodic boundary conditions are applied in the $y$ and $z$ dimensions, with electrodes at $x = 0$ and $x = 64$

nm, parallel to the *y-z* plane. Voxels are labelled as either acceptor (*n*) or donor (*p*), with a 1:1 ratio in every morphology.

Disordered blend morphologies with increasing feature size were created from the Ising model.[9] Interdigitated rod structures of different widths were produced in a chessboard layout. Triply-periodic bicontinuous morphologies were derived from the gyroid and diamond triply-periodic minimal surfaces of cubic symmetry.[37,38] These surfaces have vanishing mean curvature, are periodic in three perpendicular directions and divide space into two identical labyrinth-like domains each of which represents a continuous tunnel network extending periodically throughout space. The gyroid and the diamond surfaces are examples of triply-periodic minimal surfaces that are structural models for certain mesophases in copolymer blends and surfactant/lipid mixtures.[39] A full descriptions of how these morphologies have been created has been included in the supporting information. Scaled down versions of each structure were used as a unit cell for larger, multiply-connected structures to creating morphologies of the same volume but varying $l_f$, 1, panel (f). For comparison, a bilayer structure is also studied.

Excitons enter the system at a rate determined by the absorption profile and execute a random walk in the phase in which they are created at a hopping rate determined by **Förster theory**[40]

$$w_{ij} = w_{ex} \left( \frac{R_0}{R_{ij}} \right)^6 f(E_i, E_j) \tag{1}$$

where $R_{ij}$ is the distance between hopping sites $i$ and $j$ and $R_0$ is the Förster radius. $E_i$ and $E_j$ are the energies of sites $i$ and $j$. The attempt to hop frequency $w_e R_0^6$ represents an average of inter- and intra-chain hopping. **We do not distinguish between inter- and intra-chain exciton or charge motion as it is hard to ascertain how the chains pack together. Not accounting for the full chain picture also saves considerably on computing time whilst still allowing us to examine the parameters of interest.**

The factor

$$f(E_i, E_j) = \exp\left( -\frac{E_j - E_i}{k_B T} \right) \quad E_j > E_i \quad , \quad f(E_i, E_j) = 1 \quad E_j < E_i \quad . \tag{2}$$

describes the influence of site energies on hopping rate. $E_i$ and $E_j$ are determined from
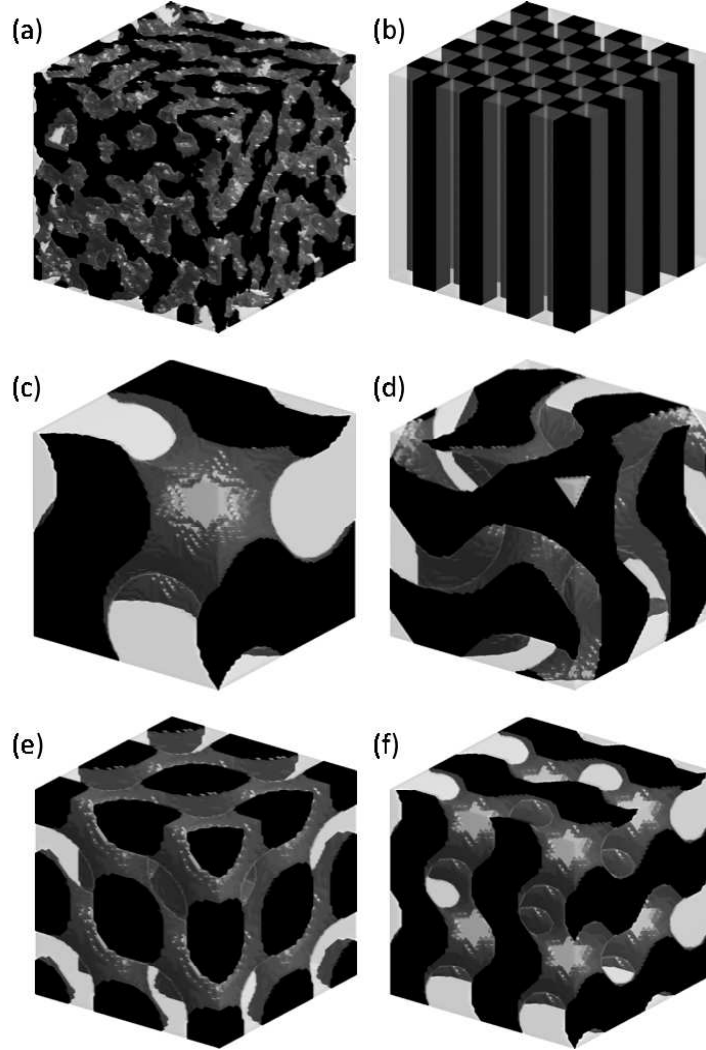
Figure 1: Disordered blend (a) and interdigitated rod (b) structures. Panels (c-e) show a single cubic translational unit cell of the single gyroid with symmetry $I4_132$ (c), the $Ia\overline{3}d$ double gyroid (d) and the $Pn\overline{3}m$ double diamond (e) structures. Panel (f) shows an extended gyroid structure consisting of $2^3$ translational unit cells of the structure in (c) with half the lattice length $a$.

a Gaussian distributed density of states (DOS) of width $\sigma$, which describes material disorder. For simplicity, the same density of states is used for both charges and excitons. Instead of hopping, the exciton may recombine at a rate of $\tau_{ex}^{-1}$.

If an exciton encounters an interface between the $n$- and $p$-type polymer, a charge transfer state (bound charge pair) may be created at a rate of $k_{diss}$. This state can form a geminate electron-hole pair or recombine at a rate $k_r$, at which point it is considered

6

to be lost from the system.[13]

The charges created by exciton dissociation or by injection are allowed to hop from sites $i$ to $j$ where site $j$ is a nearest neighbour of the same polymer as site $i$ at a rate obtained from Marcus theory,[41]

$$R_{ij} = v_{hop} \exp\left[-\frac{(E_j - E_i + \lambda)^2}{4\lambda k_B T}\right] . \tag{3}$$

Here, $\lambda$ corresponds to the chain reorganisation energy and the prefactor $v_{hop}$ encompasses the electronic coupling between states and the distance between hopping sites, both of which are taken as constant for nearest-neighbour hopping in a single system.

The $i$th site is initially assigned an energy

$$E_i = E_{\sigma i} + \phi + \Delta_{inj} - eFx_i - \frac{e^2}{16\pi\varepsilon_0\varepsilon_r x_i} \tag{4}$$

where $E_{\sigma i}$ is chosen from a Gaussian distribution as noted above, $\phi$ is the work function of the Al contact, $\Delta_{inj}$ is the injection barrier, $F$ is the net field resultant from built-in voltage ($V_{bi}$) and the applied bias, $x_i$ is the distance from the contact, and the final term describes image charge effects for a material of dielectric constant $\varepsilon_0\varepsilon_r$ where $\varepsilon_0$ is the vacuum permittivity and $e$ is the electron charge magnitude. An equivalent expression exists for hole transport.

**When calculating hopping rates for charge carriers, $E_i$ and $E_j$ in Eq. 3 are further updated by a factor $\triangle E$ to take account of the coulombic effect of all other charges within the system, where**

$$\triangle E = \sum_{j=1}^{n} \frac{qe}{4\pi\varepsilon_0\varepsilon_r r_{ij}} \tag{5}$$

**where $n+1$ is the total number of charges in the system, $q = +e$ for electron-electron and hole-hole repulsion and $-e$ for electron-hole attraction and $r_{ij}$ is the distance between charges $i$ and $j$. At the charge densities seen here this approach is computationally far more efficient than updating all the sites within a specified cutoff radius of the moving charge carrier, and the number of calculations**

**scales with $n$, the number of charges. Although coulombic interactions are updated when calculating each new event, waiting times for events already held in the queue are not. This procedure saves computing time without compromising on simulation accuracy [42]**

Once a hop has occurred, the possibilities are: further hopping, geminate or bimolecular recombination, or extraction at an electrode; depending on the location of the charge within the morphology and with respect to other particles. Charges may also be injected, via a hop from the Fermi level of the electrode over the injection barrier into the first monolayer. [42,43]

Simulation of charge and exciton dynamics is carried out using the First Reaction Method (FRM) algorithm. Each event has an associated waiting time $\tau = (1/w)\ln(X)$ based on its rate $w$ and a random number $X$ uniformly distributed between 0 and 1. The events are stored in a queue in order of increasing $\tau$. At each timestep, the event at the start of the queue is executed, and then removed. The waiting times of all events remaining in the queue are then reduced by the time expired. Site energies are updated, and new events enabled and existing ones disabled as appropriate. To reduce computing resource, events which are already stored in the queue are based on an earlier state of the system even though the system may have changed significantly, an approximation validated by. [42] Simulations are allowed to continue until steady-state has been maintained for enough time to build up useful data, and are repeated to reduce uncertainty.

To characterise the morphologies at a detailed level we calculate the fraction of excitons which dissociate $\eta_{ed}$; the fraction of charges that recombine with their geminate twins $\eta_{gr}$; that recombine with other charges (bimolecular recombination) $\eta_{br}$; and that are extracted, the charge collection efficiency $\eta_{cc}$. The internal quantum efficiency (IQE) is the product $\eta_{cc} \times \eta_{ed}$. The power conversion efficiency (PCE), is the ratio of the power per unit area at the maximum power operating point delivered by the device, obtained from the current density $J_m$ and voltage $V_m$ at that point, to the incident power

8

per unit area at AM 1.5 illumination. The fill factor

$$FF = \frac{J_m V_m}{J_{SC} V_{OC}} \tag{6}$$

where $J_{SC}$ is the short-circuit current density, and $V_{OC}$ is the open-circuit voltage.

As far as possible, we take our system parameters from experimental studies of the hole transporting copolymer poly(9,9'-dioctylfluorene-co-bis(N,N'-(4,butylphenyl))bis(N,N'-phenyl-1,4-phenylene)diamine) (PFB) blended with the electron transporting copolymer poly(9,9'-dioctylfluorene-co-benzothiadiazole) (F8BT), where the hole extracting electrode is ITO/PEDOT:PSS where ITO is Indium Tin Oxide and PEDOT:PSS is Poly(3,4-ethylenedioxythiophene) poly(styrenesulfonate) and the electron extracting electrode is Al, as this system has been extensively studied.[10,44,45] From spectral data, this blend has been calculated to absorb 5.8% of the AM (air mass) 1.5 solar emission spectrum, with an assumed Gaussian optical field profile.[9] We set $w_{ex}R_0^6 = 0.02$, such that simulations of excitons in a single component material with energetic disorder $\sigma$ = 0.062 eV gives a diffusion length $L_{ex}$ of 6 nm[46] in a lifetime $\tau_{ex}$ of 500 ps.[47] Taking $\lambda = 0.75$ eV and a mobility of $\mu_0 = 1 \times 10^{-8}$ m$^2$V$s^{-1}$ for both polymers,[48,49] and by assuming isoenergetic material, we calculate $v_{hop} = 2.41$ ps$^{-1}$ using the Einstein relationship. Other parameter values are $k_{diss} = (100 \text{ fs})^{-1}$,[50] $k_r = 1 \times 10^6$ s$^{-1}$, $\varepsilon = 4$, $V_{bi}$ = 1.3 V. $\Delta_{inj} = 0.8$ eV for electrons and 0.1 eV for holes based on the HOMO/LUMO levels of the polymers and the work functions of the electrodes.[51–53] **The uncertainty in the hole injection barrier height was overcome by fitting dark current modelling to published experimental results,[45] ensuring the charge density and local field near the electrodes are correct.**

## Results and discussion

2 (a) compares the IQE of the five different morphology classes, as a function of feature size. Given the disparity in feature sizes simulated, interpolation has been used to find the peak efficiency of each morphology class shown in 1. All the morphology classes
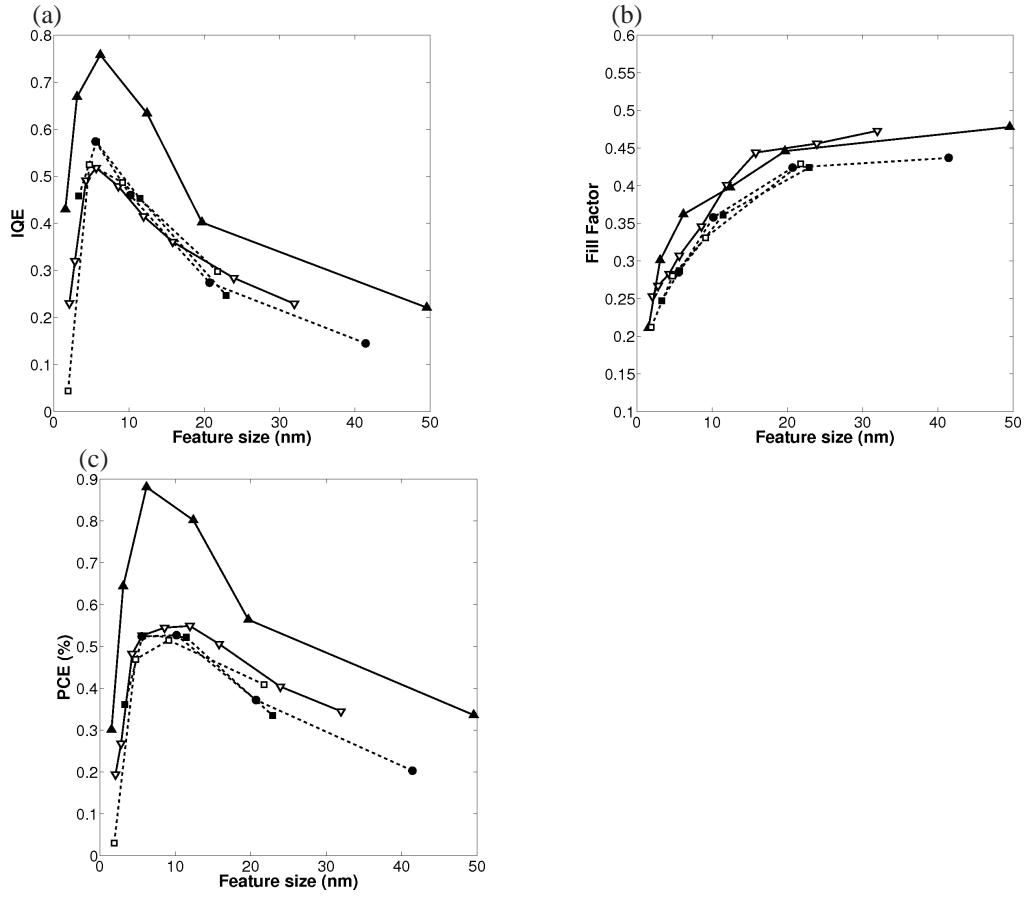
Figure 2: a) IQE, b) FF and c) PCE as a function of feature size for blends (solid line, ▽), rods (solid line, ▲), gyroids (dashed line, ●), double gyroid (dashed line, ■) and double diamond (dashed line, □).

reproduced the well-established behaviour of an idealised intermediate morphology, where the product of $\eta_{ed}$ and $\eta_{cc}$ is optimised. Morphology class has little effect on the optimum feature size, which is close to the exciton diffusion length (6 nm) in each case. Overall, the gyroid, double gyroid and double diamond structures do not compare as favourably with the disordered blend morphologies as might be expected. At the peak IQE, the bicontinuous structures are fractionally more efficient than the blend. These results are sensitive to device parameters,[9] many of which are only known approximately as they depend on chain alignments, for example the dissociation rates,[54] exciton diffusion coefficient[47] and mobilities,[55] and these alignments will vary widely in the disordered films. Another problem is domain purity as minority components in

Table 1: Interpolated peak values of IQE and PCE, and the feature size at which they occur. Fill factor values are taken at the peak PCE.

|  | IQE | PCE | FF |
|---|---|---|---|
| **Blend** | 0.55 (5.6 nm) | 0.56% (7.5 nm) | 0.34 |
| **Rod** | 0.77 (6.5 nm) | 0.91% (8.0 nm) | 0.38 |
| **Gyroid** | 0.57 (5.6 nm) | 0.53% (8.6 nm) | 0.33 |
| **Double gyroid** | 0.58 (6.8 nm) | 0.57% (8.3 nm) | 0.32 |
| **Double diamond** | 0.59 (6.4 nm) | 0.56% (6.9 nm) | 0.30 |

the blend domains can have a measurable impact on the results as they act as dissociation, and hence recombination, centres. Recent experimental studies have found that the domain size of an optimised morphology can exceed the exciton diffusion length[45] even though domain purity >90% is common.[56,57] We repeated the calculations of IQE in the blend morphologies, this time creating additional islands by swopping voxels in the domains of each polymer, and then plotted the results against the original feature sizes to mimic experiment where the islands are invisible under AFM. The peak IQE is reduced from 0.55 at a feature size of 5.6 nm to 0.50 at a feature size of 6.4 nm if 1% impurities are introduced and to 0.48 at a feature size of 7.5 nm if there are 5% impurities. The additional islands reduce the drop-off in exciton dissociation efficiency as $l_f$ increases. However, $\eta_{cc}$ no longer increases monotonically with feature size across the range of morphologies, but shows a peak because exciton dissociation preferentially takes place at the islands as the interfacial area of the charge transport pathways decreases, and such charges are unable to escape and contribute to the current. At the peak IQE, most dissociation takes place at connected features, and so the peak IQE value drops only marginally. Self-assembled nanostructures are less likely to contain these islands, enhancing their appeal.

From 2 (b), FF can be seen to increase steadily with $l_f$, in agreement with experiment,[45,58,59] due to the morphological dependence of $\eta_{cc}$. In the blends, FF is $\approx 0.25$ at the smallest feature sizes modelled, suggesting drift-only transport which produces a linear J-V curve. The features in these morphologies are so small that charges follow extremely tortuous paths. As there are interfaces close to each other throughout the device, charge generation is uniformly spread so there are only small charge gradients,

11

minimising the diffusion current. The range of FF values is similar to experimental findings[45] and for the limiting case of a bilayer structure (not shown) FF is 0.54.

2 (c) shows that PCEs are comparable for the novel structures and the blends. The feature size of the optimum morphology increases noticeably when examining complete J-V performance, compared to characterisation in terms of IQE alone, due to the morphological dependence of FF. Thus a morphology optimised at short circuit will not be the optimal morphology for power conversion. Vertical rod morphologies are consistently superior to all others examined. The lower than expected IQE values in the bicontinuous morphologies can be understood by examining the recombination data in 3.

Increasing $l_f$ may be expected to reduce geminate recombination because the charges have more room in which to escape their geminate twin. For blend morphologies, the large drop in $\eta_{gr}(l_f)$ up till 3 nm is attributed to the difficulty for an initially separated geminate pair at the smallest separations to escape their mutual coulombic well. At $l_f =3$ nm there is a sharp change in the drop off rate for $\eta_{gr}(l_f)$. For $l_f > 3$nm, charges can avoid recombination, but $\eta_{gr}(l_f)$ decreases further because the blend structure morphology can force charges back together en route to the electrodes. As $l_f$ continues to increase, the charges have more room in which to escape their geminate twin so $\eta_{gr}$ is less sensitive to $l_f$. Such behaviour was seen and explained by Groves et. al.[13] for bilayer and blend devices. Single and double gyroid structures, however, exhibit an increase in $\eta_{gr}$ with $l_f$ for $l_f > 3$nm, an effect which will be discussed below with reference to illumination level.

It is not possible to create the single gyroid and double diamond morphologies for $l_f$ under 2 nm, but for the other morphologies, $\eta_{br}$ takes its lowest values at these small feature sizes, as can be seen in 3(b). This result is a consequence of $\eta_{gr}$ being large for these morphologies, removing charges that could otherwise suffer bimolecular recombination. Once $\eta_{gr}$ reaches a low value as $l_f$ approaches 3 nm, there is a sharp increase in $\eta_{br}$. For $l_f> 3$ nm $\eta_{br}$ drops off for all morphologies, although the single gyroid shows slightly less bimolecular recombination than the blends at larger feature sizes. Increasing $l_f$ reduces the probability of an exciton reaching an interface and

dissociating, lowering the charge density. It also increases the average distance between domains, so that dissociated charges are less likely to encounter other charges of the opposite type after escaping their geminate twins. In [14] $\eta_{br}$ was predicted for different feature sizes with related conclusions.

In general the novel morphologies appear to be no better than blends at either achieving separation of the geminate pair, or preventing recombination en route to the electrodes. We infer that the presence of islands as well as discontinuous and 'cul-de-sac' pathways in the blends is not a severe limitation in their efficiency. Rod structures exhibit a much lower level of geminate recombination at almost every feature size. This advantage is lost at the two smallest rod sizes, 1 nm and 2 nm, because, as for the smallest blend structures, motion perpendicular to the interface is tightly constrained so separation is highly unlikely, as charges are unable to escape their mutual coulombic well. In this case interfacial tracking is more likely to occur, increasing the number of recombination attempts. However, the short pathways for extraction in the rod structures ensures bimolecular recombination is minimal even for the narrowest rods, where charges created within different rods can also remain entirely isolated from one another. Furthermore, unlike the novel structures, charges in the rod structures only move parallel to the field with a direct route to the electrodes, reducing escape time.

To further characterise the bicontinuous morphologies with respect to the other structures, the same simulations were performed at 5 suns illumination, to examine the influence of high charge densities on performance. The polymers simulated here have low absorption coefficients, so the charge densities at this much higher illumination level show effects that may be seen in other materials at 1 sun. The IQEs for the different morphology classes and the geminate and bimolecular recombination levels are given in Figures 1-3 of the supporting information, and can be compared to 2 (a) and 3(a) and (b). We find that geminate recombination is decreased by up to 25% for the blends and novel structures, but increases fractionally for the rod structures. We attribute this decrease to diffusion away from curved surfaces, which cannot occur in the rod structures. However, the decreased geminate recombination does not result in an increased FF or IQE, as $\eta_{br}$ increases by a factor of 2 to 3, making it a loss

process now comparable to the geminate mechanism. This result leads to a decrease in the efficiency of the blends and bicontinuous structures by 12-25%, but the rods by only 8%, widening their advantage over the other structures. In the blends, the peak IQE shifts from the 5.6 nm to 8.6 nm morphology as wider pathways are required to keep recombination at a reasonable level. We can conclude, then, that the novel structures are no better at handling higher charge densities than the blends. The level of bimolecular recombination increases by the same amount, further evidence that the disordered structure of the blends is not primarily responsible for their inefficiency.

As already mentioned, at normal illumination the gyroid and double gyroid structures exhibit an increase in $\eta_{gr}$ with $l_f$, a trend which we now see in the blend structures at 5 suns illumination when $l_f >\approx 10$ nm. We speculate that this increase occurs because **the effect on the local field of** the presence of multiple charge pairs along the same planar stretch of interface interferes with charge separation, an effect which occurs more strongly for larger domains. The existence of this effect is confirmed by intensity dependent simulations up to 10 suns (not shown) of the bilayer and rod structures, where all the surfaces are planar. We find that $\eta_{gr}$ increases with illumination, though more weakly for the rods due to the greater surface area. We have already seen that, at 1 sun illumination, this effect is absent in the blends but present in the gyroid and double gyroid structures. Additional simulations show the effect is absent in the latter structures at 0.01 suns, so we deduce that the influence of neighbouring geminate pairs on the attraction felt by charges within a geminate pair becomes important for the single and double gyroid structures at a lower illumination level than the blends.

**The charge densities simulated here are of the order of $10^{21}$ - $10^{22}$ m$^{-3}$, consistent with other models,** [17,44,60] **which in a system of this size consists of no more than approximately 10 charge pairs at any time. Animations show that these charge pairs remain in the viscinity of each other for a long time after dissociation, and can track each other within the device. The reason the novel morphologies are more influenced by this effect is due to the continuous nature of their interface, which allows charge pairs to track each other throughout the device, whereas the blends have broken interfaces which reduce tracking.** This effect competes with the

two already described: difficulty in escaping the mutual coulombic well at very small feature sizes, and diffusion from curved surfaces.

It is surprising that rods perform so much better than blends, whereas the novel morphologies are, at best, only marginally better. Rods have the shortest charge transport pathways, and at small feature sizes can keep charges entirely isolated from each other. However, this effect does not sufficiently explain the large difference in geminate recombination levels. In the simulation, the probability of separation following dissociation is determined by the competition between the field dependent rate for one of the charges to hop away from the interface and the constant recombination rate $k_r$. Eq. 3 shows that parallel and anti-parallel hops with respect to the field result in equal and opposite changes in the hopping rate, and hence the probability of recombination. For rods, separation is always perpendicular to the field. Blends and bicontinuous structures have interfaces at angles from 0 (field-assisted separation) to 180 degrees (field impaired separation) with respect to the field and so might be expected to have a similar efficiency to the rods. However, initially separated charges will have multiple attempts at geminate recombination if initial separation is against the field, as they will need to explore the interface to find a way out. Thus, the detrimental effect of an interface where separation is against the field, when compared to perpendicular separation, is far greater than the advantage of separation with the field.

To confirm this argument, bilayer structures were created for separation at different angles $\theta$ to the field $F$. The fraction of charges successfully escaping geminate recombination, $\eta_{gs}$, were obtained for $F = 1 \times 10^7$ Vm$^{-1}$. The results are $\eta_{gs} =$ 78%,74%,17% for $\theta = 0$, 90 and 180 degrees respectively in agreement with.[13] The magnitude of this effect shows it is the dominant limiting mechanism for efficiency. Hence, as the interfaces in the blend and bicontinuous morphologies have no preferred direction with respect to the field, the results can be expected to be noticeably below those for the rods, where $\theta$ is always 90 degrees, as we find. We do not anticipate this to be a problem when implementing these structures in DSCs, as the device structure screens out the internal field.

We can conclude that bicontinuous, triply-periodic minimal surface morphologies
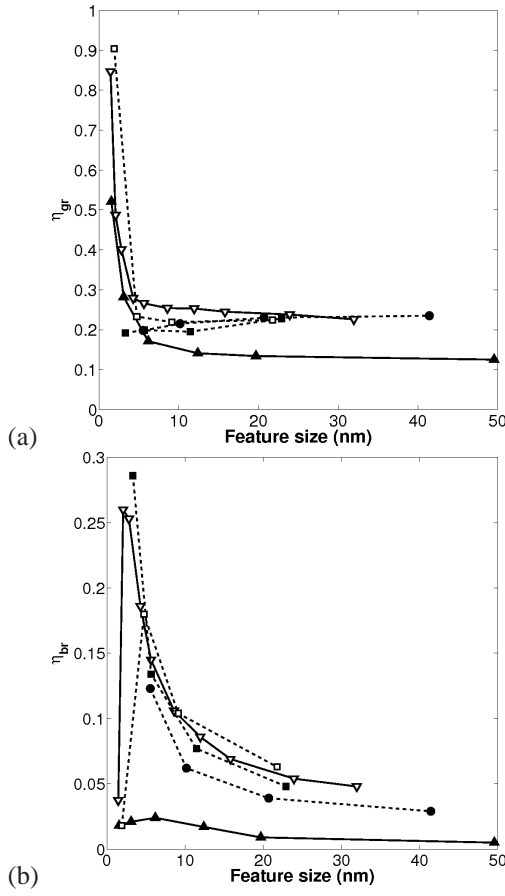
Figure 3: Recombination fraction of geminate pairs $\eta_{gr}$ (a) and of nongeminate pairs, bimolecular recombination, $\eta_{br}$ (b) for all morphology classes, as a function of feature size. Symbols and line types as for 2.

may not enhance polymer blend solar cell efficiency as much as hoped. However, optimised bicontinuous structures could be made to have higher efficiencies than blends with an optimal morphology, and the reproducibility of these structures further enhances their practical appeal. Vertical rod structures may be the best option if they can be made defect free, as they exhibit a far superior performance, A very narrow rod structure is the most desirable, to improve the exciton dissociation efficiency. In order to maintain good charge collection, high mobility materials would be required, in order to reduce geminate recombination and evacuate charges quickly to avoid subsequent loss. We hope that this paper will stimulate further measurements on cells based on bicontinuous morphologies, whether by using diblock copolymers or hybrid

16

organic/inorganic cells. Finally, whilst the biggest limitation to solar cell efficiency is likely to be optical absorption, more highly absorbing polymers are of little use if their structure and chemical properties are not tailored to handle the increased charge density efficiently.

## Acknowledgements

## Supporting information

Descriptions of how gyroid and diamond triply-periodic minimal surfaces have been created along with IQEs and the geminate and bimolecular recombination levels at 5 suns illumination. This material is available free of charge via the Internet at http://www.rsc.org.

## References

[1] M. Grätzel, *Phil. Trans. R. Soc. A: Mathematical, Physical and Engineering Sciences*, 2007, **365**, 993–1005.

[2] S. Günes, H. Neugebauer and N. Sariciftci, *Chem. Rev.*, 2007, **107**, 1324–1338.

[3] S. Günes and N. S. Sariciftci, *Inorganica Chimica Acta*, 2007, **361**, 581–8.

[4] M. Reyes-Reyes, K. Kim, J. Dewald, R. López-Sandoval, A. Avadhanula, S. Curran and D. Carroll, *Nanotechnology*, 2004, **15**, 1317.

[5] C. Ko, Y. Lin, F. Chen and C. Chu, *Applied Physics Letters*, 2007, **90**, 063509.

[6] K. Kim, J. Liu, M. Namboothiry and D. Carroll, *Appl. Phys. Lett.*, 2007, **90**, 163511.

[7] T. Kietzke, H. Horhold and D. Neher, *Chem. Mater*, 2005, **17**, 6532–7.

[8] E. Zhou, X. Zhan, X. Wang, Y. Li, S. Barlow and S. Marder, *Applied Physics Letters*, 2008, **93**, 073309.

[9] P. Watkins, A. Walker and G. Verschoor, *Nano Lett*, 2005, **5**, 1814–1818.

[10] R. Marsh, C. McNeill, A. Abrusci, A. Campbell and R. Friend, *Nano Lett*, 2008, **8**, 1393–1398.

[11] F. Yang and S. Forrest, *ACS Nano*, 2008, **2**, 1022–32.

[12] L. Meng, Y. Shang, Q. Li, Z. Shuai, R. Kimber and A. Walker, *Journal of Physical Chemistry C (Submitted)*, 2009.

[13] C. Groves, R. Marsh and N. Greenham, *J. Chem. Phys.*, 2008, **129**, 114903.

[14] C. Groves and N. Greenham, *Physical Review B*, 2008, **78**, 15.

[15] G. Buxton and N. Clarke, *Physical Review B*, 2006, **74**, 85207.

[16] C. Martin, V. Burlakov, H. Assender and D. Barkhouse, *Journal of Applied Physics*, 2007, **102**, 104506.

[17] J. Williams and A. Walker, *Nanotechnology*, 2008, **19**, 424011.

[18] A. Morteani, P. Sreearunothai, L. Herz, R. Friend and C. Silva, *Phys. Rev. Lett.*, 2004, **92**, 247402.

[19] D. Hajduk, P. Harper, S. Gruner, C. Honeker, G. Kim, E. Thomas and L. Fetters, *Macromolecules*, 1994, **27**, 4063–4075.

[20] M. Impéror-Clerc, *Current Opinion in Colloid & Interface Science*, 2005, **9**, 370–376.

[21] L. Ellison, D. Michel, F. Barmes and D. Cleaver, *Phys. Rev. Letts.*, 2006, **97**, 23.

[22] S. Sun, C. Zhang, A. Ledbetter, S. Choi, K. Seo, C. Bonner Jr, M. Drees and N. Sariciftci, *Appl. Phys. Letts*, 2007, **90**, 043117.

[23] V. N. Urade, T.-C. Wei, M. Tate, J. D. Kowalski and H. W. Hillhouse, *Chem. Mater.*, 2007, **19**, 768–7.

[24] C. Oey, A. Djurišić, H. Wang, K. Man, W. Chan, M. Xie, Y. Leung, A. Pandey, J.-M. Nunzi and P. Chu, *Nanotechnology*, 2006, **17**, 706–13.

[25] E. Crossland, M. Kamperman, M. Nedelcu, C. Ducati, U. Wiesner, D. Smilgies, G. Toombes, M. Hillmyer, S. Ludwigs, U. Steiner and H. J. Snaith, *Nano Letts*, 2009, **9**, 2807–12.

[26] E. Crossland, M. Nedelcu, C. Ducati, S. Ludwigs, M. Hillmyer, U. Steiner and H. Snaith, *Nano Letts*, 2009, **9**, 2813–19.

[27] Y. Chiba, A. Islam, Y. Watanabe, R. Komiya, N. Koide and L. Han, *Japanese J of Applied Physics Part 2 Letters*, 2006, **45**, 638.

[28] Y. Zhang, K. Tajima, K. Hirota and K. Hashimoto, *J. Am. Chem. Soc.*, 2009, **130**, 7812–3.

[29] F. Bates and G. Fredrickson, *Physics Today*, 1999, **52**, 32–39.

[30] J. Kim, *Pure and applied chemistry*, 2002, **74**, 2031–2044.

[31] B. Sumpter, M. Drummond, W. Shelton, E. Valeev and M. Barnes, *Computational Science and Discovery*, 2008, **1**, 015006.

[32] S. Sun, *Solar energy materials and solar cells*, 2003, **79**, 257–264.

[33] G. Schröder-Turk, A. Fogden and S. T. Hyde, *Eur. Phys. J. B*, 2007, **59**, 115–26.

[34] G. Schröder, S. J. Ramsden, A. Christy and S. Hyde, *The European Physical Journal B-Condensed Matter*, 2003, **35**, 551–564.

[35] J.-F. Thovert, F. Yousefian, P. Spanne, C. G. Jacquin and P. M. Adler, *Phys. Rev. E*, 2001, **63**, 061307.

[36] W. Mickel, S. Münster, L. Jawerth, D. Vader, D. Weitz, A. Sheppard, K. Mecke, B. Fabry and G. Schröder-Turk, *Biophys. J.*, 2008, **95**, 6072–6080.

[37] H. Schwarz, *Gesammelte Mathematische Abhandlungen. 2 Bände.*, Springer, Berlin, 1890.

[38] A. H. Schoen, *Infinite Periodic Minimal Surfaces without Self-Intersections*, NASA Technical Report TN D-5541, 1970.

[39] S. T. Hyde, S. Andersson, K. Larsson, Z. Blum, T. Landh, S. Lidin and B. W. Ninham, *the language of shape*, elsevier science b. v., amsterdam, 1st edn., 1997.

[40] V. May and O. Kühn, *Charge and energy transfer dynamics in molecular systems*, Vch Verlagsgesellschaft Mbh, 2001.

[41] R. Marcus, *Reviews of Modern Physics*, 1993, **65**, 599–610.

[42] N. C. G. R. A. Marsh, C. Groves, *J. Appl.Phys.*, 2007, **101**, 083509.

[43] U. Wolf, V. Arkhipov and H. Bässler, *Physical Review B*, 1999, **59**, 7507–7513.

[44] J. Barker, C. Ramsdale and N. Greenham, *Phys. Rev. B*, 2003, **67**, 075205.

[45] C. McNeill, S. Westenhoff, C. Groves, R. Friend and N. Greenham, *J. Phys. Chem. C*, 2007, **111**, 19153–19160.

[46] D. Markov, E. Amsterdam, P. Blom, A. Sieval and J. Hummelen, *Journal of Physical Chemistry A*, 2005, **109**, 5266–74.

[47] S. Athanasopoulos, E. Hennebicq, D. Beljonne and A. Walker, *J. Phys. Chem. C*, 2008, **112**, 11532–8.

[48] A. Campbell, D. Bradley and H. Antoniadis, *Applied Physics Letters*, 2001, **79**, 2133.

[49] R. A. Khan, D. Poplavskyy, T. Kreouzis and D. Bradley, *Physical review B. Condensed matter and materials physics*, 2007, **75**, 035215.

[50] C. Brabec, N. Sariciftci and J. Hummelen, *Advanced Functional Materials*, 2001, **11**, 15–26.

[51] T. Brown, J. Kim, R. Friend, F. Cacialli, R. Daik and W. Feast, *Applied Physics Letters*, 1999, **75**, 1679.

[52] E. Moons, *Journal of Physics Condensed Matter*, 2002, **14**, 12235–12260.

[53] J. Lee, *Applied Physics Letters*, 2006, **88**, 073512.

[54] Y. Huang, S. Westenhoff, I. Avilov, P. Sreearunothai, J. Hodgkiss, C. Deleener, R. Friend and D. Beljonne, *Nature Materials*, 2008, **7**, 483–489.

[55] S. Athanasopoulos, J. Kirkpatrick, D. Martinez, J. Frost, C. Foden, A. Walker and J. Nelson, *Nano Lett*, 2007, **7**, 1785–1788.

[56] T. Kietzke, D. Neher, M. Kumke, O. Ghazy, U. Ziener and K. Landfester, *Small*, 2007, **3**, 1041–8.

[57] C. McNeill, B. Watts, L. Thomsen, H. Ade, N. Greenham and P. Dastoor, *Macromolecules*, 2007, **40**, 3263–3270.

[58] J. van Duren, X. Yang, J. Loos, C. Bulle-Lieuwma, A. Sieval, J. Hummelen and R. Janssen, *Advanced Functional Materials*, 2004, **14**, 425–434.

[59] W. Ma, C. Yang, X. Gong, K. Lee and A. Heeger, *Advanced Functional Materials*, 2005, **15**, 1617–1622.

[60] L. J. A. Koster, E. C. P. Smits, V. D. Mihailetchi and P. W. M. Blom, *Phys. Rev. B*, 2005, **72**, 85205.